BMC Gastroenterology

RESEARCH

Open Access

ZBTB10 as a potential prognosis biomarker and correlates with the tumor immune microenvironment in stomach adenocarcinoma

Yingdi Jiang[1†], Fuhua Han[2†], Lu Dai[3†], Shali Qiu[4], Yanjie Zhou[1], Ke Wang[5*] and Jiang Lin[1*]

Abstract

Background ZBTB10 is a member of the zinc finger and bric-a-brac/tramtrack/broad (ZBTB) domain-containing protein family, reported to be associated with tumorigenesis and progression. However, its specific roles in oncogenesis, prognosis, and immune infiltration in stomach adenocarcinoma (STAD) remain to be elucidated.

Methods We analyzed ZBTB10 mRNA and protein expression profiling in STAD tissues using various bioinformatics tools, including TIMER2, GEO, Human Protein Atlas (HPA) databases, and R software. Survival analysis was performed through the Kaplan–Meier plotter. UALCAN and TCGA databases were used to evaluate the association of ZBTB10 expression with clinicopathological characteristics. Genetic alterations of ZBTB10 in human tumor samples were analyzed using the cBioPortal database. The correlation between ZBTB10 expression and immune cell infiltration was assessed using the TISIDB and CIBERSORT algorithms. Gene Set Enrichment Analysis (GSEA) and Kyoto Encyclopedia of Genes and Genomes (KEGG) pathway were applied to investigate the potential mechanism of ZBTB10 in STAD. Additionally, in vitro assays such as CCK-8, colony formation, and wound healing assays were performed to determine the biological role of ZBTB10 in STAD cells. Multiple immunohistochemistry (mIHC) was applied to characterize the association between immune cell infiltration and ZBTB10 expression in STAD tumor tissues.

Results Overall, ZBTB10 was differentially expressed in STAD compared to adjacent normal tissues, and higher ZBTB10 expression correlated with poorer overall survival (OS). Furthermore, GSEA and KEGG analysis suggested that ZBTB10 was predominantly involved in focal adhesion, PI3K-Akt signaling, and MAPK signaling pathways, suggesting its potential role in promoting tumor growth and progression. Moreover, based on the CIBERSORT algorithm, the expression of ZBTB10 was positively related to the levels of B cells, CD4 + T cells, M1 macrophages, and neutrophil cells. Meanwhile, ZBTB10 expression appeared to be negatively associated with tumor mutation burden (TMB) and microsatellite instability (MSI) in STAD, both of which influenced the efficacy of tumor immunotherapy. In vitro experiments demonstrated that ZBTB10 knockdown significantly inhibited tumor cell proliferation and invasion,

[†]Yingdi Jiang, Fuhua Han and Lu Dai contributed equally to this work.

*Correspondence:
Ke Wang
jywke@163.com
Jiang Lin
15086265@qq.com
Full list of author information is available at the end of the article

and organoid area in STAD cell lines. The immune cell signature of CD45 was more prevalent with ZBTB10 expression in tumor tissue sections compared to adjacent normal tissues from STAD patients.

Conclusions Upregulated ZBTB10 is significantly correlated with poor survival outcomes and immune infiltration in STAD, revealing that ZBTB10 may serve as a promising prognostic biomarker and a potential target for immunotherapy in STAD.

Keywords STAD, ZBTB10, Prognosis, Immune infiltration

Introduction

Stomach adenocarcinoma (STAD) is one of the most common malignancies worldwide, causing approximately 660,000 deaths per year and ranking as the fourth leading cause of cancer-related death [1–3]. Currently, the management of STAD primarily includes endoscopic detection, followed by gastrectomy and chemoradiotherapy [4, 5]. Despite advancements in next-generation sequencing (NGS) and large-scale high-throughput molecular profiling studies have provided crucial insights into STAD, as well as the remarkable achievements in targeted therapy and immunotherapy [4, 6], the 5-year survival rate for STAD remains exceptionally low, at only 36.4% after treatment [7]. Therefore, there is an urgent need to identify novel biomarkers to improve the prognosis of STAD. ZBTB proteins belong to zinc finger proteins (ZFPs) and BTB Domain-containing protein family, linked to immune infiltration, cell differentiation, and tumorigenesis [8–10]. ZFPs, such as ZBTB27, ZBTB9, and ZBTB33 participate in the regulation of DNA damage response, cell cycle progression, DNA methylation, and drug resistance [11, 12]. ZBTB10 is a member of the ZBTB protein family, predominantly localizes to the nucleoplasm [13]. Several studies have suggested that ZBTB10 serves as a tumor suppressor in breast and colon cancers by repressing specificity protein (Sp) transactivation, which in turn inhibits tumor growth, chemoresistance and metastasis [14, 15]. Additionally, ZBTB10 has been reported as a target of miR-27a, downregulating the expression of vascular endothelial growth factor (VEGF), Cox-2 and survivin, thereby influencing tumor angiogenesis in ovarian cancer [16]. Furthermore, ZBTB10 is also crucial for dendritic cell (DC) activation and cytokine secretion, inducing immunogenic responses in conventional type 1 dendritic cells (cDC1) by regulating NF-κB signaling and nuclear translocation [17]. Nevertheless, the role of ZBTB10 in stomach adenocarcinoma (STAD) remains poorly studied and requires further investigation. In this study, we performed a comprehensive analysis of ZBTB10 expression and prognostic value in STAD patients by utilizing multiple public databases and functional assays. Our findings revealed that ZBTB10 is significantly overexpressed in STAD tissues compared to adjacent normal tissues, and its high expression correlates with poor clinical outcomes. Moreover, we uncovered a potential link between ZBTB10 expression and the tumor immune microenvironment, offering novel insights into the molecular mechanisms of STAD.

Materials and methods

Data collection and differential expression analysis

Gene expression profiles and clinical information of a total 375 tumor samples of STAD and 32 adjacent normal samples were downloaded from the Cancer Genome Atlas (TCGA) (https://portal.gdc.cancer.gov/). Additionally, the RNA-seq data from GSE54129 and GSE79973 were obtained from the Gene Expression Omnibus (GEO) (https://www.ncbi.nlm.nih.gov/). The expression data were normalized, then transformed into TPM format and $\log_2$ conversion for further study. Tumor Immune Estimation Resource 2.0 (TIMER2) (http://timer.cistrome.org) was employed to obtain the expression landscape of ZBTB10 across various cancers and adjacent normal tissues. The UALCAN database (http://ualcan.path.uab.edu/index.html) was used to analyze publicly available cancer information, including TCGA gene expression and clinical data, and to compare the transcription levels of ZBTB10 across clinical characteristics in STAD, such as subtypes, substages, and TP53 mutation status. The Human Protein Atlas (HPA) (https://www.proteinatlas.org/) contains the protein expression profiles for both tumors and normal tissues. In this study, we utilized the HPA database to compare the protein expression levels of ZBTB10 between normal tissues and STAD tissues. The CCLE database (https://sites.broadinstitute.org/ccle), a large cancer genome information database, was utilized to analyze the mRNA expression of ZBTB10 in STAD cell lines.

Diagnostic and prognostic analysis

The survival receiver operating characteristic (ROC) curve analysis was performed to estimate the predictive accuracy of ZBTB10 expression with survival times. Kaplan–Meier survival analysis (http://kmplot.com) was conducted to evaluate the prognostic value of ZBTB10 at the mRNA level in STAD. Additionally, the hazard ratio (HR), 95% confidence interval (95% CI), and log-rank p-value were calculated.

Genetic alterations and prognostic analysis

cBioPortal (https://www.cbioportal.org/) includes comprehensive information on DNA methylation, non − synonymous mutations, and DNA copy number data. It was applied to explore the mutation site and frequency of ZBTB10, as well as to evaluate the prognostic value of ZBTB10 alterations in STAD using TCGA data. Tumor mutation burden (TMB), a quantifiable biomarker that reflects the number of mutations within tumor cells. Microsatellite Instability (MSI), an indicator of DNA mismatch repair defects, was obtained from the TCGA database. The "maftools" R package was applied to analyze the relationship between ZBTB10 expression and both TMB and MSI by Spearman's rank correlation coefficient.

Immunocytes infiltration analysis

TISIDB (http://cis.Hku.hk/TISIDB/) is an online repository portal for tumor and immune system interaction. In this study, TISIDB was utilized to analyze the correlation between ZBTB10 and tumor-infiltrating lymphocytes (TILs), immunostimulators, and immunoinhibitors in STAD. CIBERSORT (https://cibersort.stanford.edu/) is a deconvolution algorithm using gene expression profiles to characterize the composition of immune cells. It was employed to estimate the relative abundance of 22 infiltrating immune cells based on ZBTB10 expression in STAD tissues. Additionally, the ESTIMATE algorithm was used to calculate immune and stromal scores for gene expression profiles in each tumor sample [18]. In this study, we analyzed the relationship between ZBTB10 expression and these scores according to the immune purity of the expression matrix using the "estimate" R package.

Associated genes' function analysis

We obtained RNA sequencing data of STAD patients from the TCGA database to identify differentially expressed genes (DEGs). Patients were separated into experimental groups (ZBTB10 ^{high}) and control groups (ZBTB10 ^{low}) based on the median ZBTB10 expression level in STAD, and DEGs were identified according to the threshold of |log2 fold change|> 0.5 and an adjusted p-value < 0.05. Finally, the 1979 upregulated or downregulated genes were collected and utilized as the ZBTB10-related signature. Gene Ontology (GO) and Kyoto Encyclopedia of Genes and Genomes (KEGG) pathway analysis were applied to assess ZBTB10-related DEGs in STAD, which revealed the function of DEGs in the biological process, molecular function, and pathways. The clusterProfiler and "ggplot2" R packages were utilized for the visualization of enriched pathways.

Gene set enrichment analysis

The gene set enrichment analysis (GSEA) was performed to investigate the potential pathogenic mechanisms of ZBTB10 in STAD through clusterProfiler package. The gene set (h.all.v7.2.symbols.gmt) was obtained from the Molecular Signatures Database. Patients were separated into ZBTB10 ^{high} and ZBTB10 ^{low} control groups according to the median expression level of ZBTB10, and differentially expressed genes were subsequently enriched based on the Hallmark gene set. The normalized enrichment score (NES) >1 and false discovery rate (FDR) < 0.05 were considered significant enrichment.

Analysis of gene co-expression with ZBTB10

The top 100 co-expressed genes of ZBTB10 from the cBioPortal database were acquired and submitted into STRING (https://cn.string-db.org/) to construct the protein–protein interaction (PPI) network. The results were visualized using Cytoscape software. Gene ontology (GO) enrichment analyses were performed to investigate co-expressed genes using the R package "clusterProfiler".

Cell culture

Human gastric cancer cell line AGS and MKN-45 were obtained from the Shanghai Institute of Cell Biology, Chinese Academy of Sciences (Shanghai, China) and cultured in RPMI-1640 medium (Servicebio, Wuhan, China) supplemented with 10% fetal bovine serum (FBS, Biological Industries, Beit-Haemek, Israel) and 1% penicillin and streptomycin (P/S; Hyclone). Cells were maintained at 37 °C in a humidified atmosphere with 5% CO_2.

RNA interference and transfection

The small interfering RNA (siRNA) targeting human ZBTB10 was synthesized by Jima, Inc., with the sequence 5'-GGCCAAAUGAGAACUCUUATT-3'. Scrambled sequences were used as a negative control. Cells at 70–80% confluence were transfected using Lipofectamine 2000 reagent (Invitrogen, Carlsbad, USA) following the manufacturer's instructions. Transfection complexes were added directly to the cells at a final concentration of 100 nM siRNA. For qPCR analysis, total RNA was extracted at 72 h after transfection.

Quantitative real-time polymerase chain reaction (qRT-PCR)

RT-PCR was used to detect mRNA expression after interfering with ZBTB10. Total RNA was extracted from cells using Trizol reagent (Sigma, USA) following the manufacturer's protocol, and 2 μg of RNA was reverse-transcribed into cDNA using the HiScript Synthesis Kit

(CoWin Bioscience, China). qPCR was performed to detect relative mRNA expression using Real SYBR Mixture (CoWin Bioscience, China). GAPDH served as a loading control. The primer sequences for PCR were as follows:

GAPDH(F): 5'- GTCTCCTCTGACTTCAACAGCG- 3'.
GAPDH (R): 5'- ACCACCCTGTTGCTGTAGCCAA- 3'.
ZBTB10 (F): 5'- GCTGGATAGTAGTTATGTTGC- 3'.
ZBTB10 (R): 5'- CTGAGTGGTTTGATGGACAGA- 3'.

Western blot

Total proteins were collected from cells using RIPA lysis buffer and protein concentration was quantified by BCA Protein Assay Kit (CWBIO, China). Equal amounts of protein (30 μg per lane) were then separated by 10% SDS–polyacrylamide gel electrophoresis (PAGE) and subsequently transferred to PVDF membranes. The membranes were then blocked with 5% non-fat milk at room temperature for 1 h, followed by incubation with primary antibodies against ZBTB10 (1:1000, Proteintech, China) and GAPDH (1:1000, Abcam) overnight at 4 °C. After washing with TBST, the membranes were incubated with HRP-conjugated secondary antibodies at room temperature for 1 h. Protein bands were visualized by chemiluminescence.

Cell growth assay and colony formation assay

Cell growth was assessed using the Cell Counting Kit-8 Assay Kit (Bimake, Houston, TX) according to the manufacturer's protocol. Briefly, the density of cells was adjusted to 1000 cells/well and cultured in 96-well plates for 2 h to allow cells to attach to the bottom of the wells, then 10 μL CCK-8 solution was added to each well at indicated time points (0 h,24 h,48 h,72 h). Cell growth was determined by measuring the absorbance of OD450. For the colony formation assay, 1000 indicated cells were seeded into six-well plates and maintained in medium containing 10% FBS for 14 days. The colonies were then fixed with 4% paraformaldehyde (PFA) (Sangon, Shanghai, China) and stained with 0.1% crystal violet (Sangon, China). The number of colonies > 50 cells was counted using an inverted microscope.

Generation and maintenance of gastric organoids

Clinical samples used for gastric organoids were obtained from STAD patients of Jiangyin Hospital of Xuzhou Medical University with patients' informed consent. Gastric glands from tumors and normal tissues were isolated for organoid culture as previously described [19, 20]. Briefly, tissues were first minced and washed in PBS, and then dissected into smaller pieces and incubated in a PBS-based chelation buffer (10 mM EDTA; 0.5 mM DL-dithiothreitol, Thermo Fisher Scientific; 1× Penicillin/Streptomycin; 10 μM Y-27632, Stem Cell Technologies; and 100 μg/mL primocin, Thermo Fisher Scientific) at 4 °C for 1 h, and finally shaken vigorously by hands. After shaking, the released glands were collected by centrifugation at 600 ×g for 5 min, washed three times with PBS, and once with advanced DMEM/F12 (Thermo Fisher Scientific). Afterward, the gastric glands were seeded into ultra-low attachment 6-well culture plates (Corning). Gastric organoid cultures were maintained in culture medium including advanced DMEM/F12, 1× Penicillin/Streptomycin, 1× HEPES (Thermo Fisher Scientific), 1× Glutamax (Thermo Fisher Scientific), 50 ng/mL EGF (Thermo Fisher Scientific), 10% Noggin conditioned medium (Thermo Fisher Scientific), 10% Rspo1 conditioned medium (Thermo Fisher Scientific), 50% Wnt-3 A conditioned medium (Thermo Fisher Scientific), 100 ng/mL of FGF10 (Thermo Fisher Scientific), 1 nM of Gastrin (Thermo Fisher Scientific), 1× B27 (Thermo Fisher Scientific) and 1 mM N-acetylcysteine (Thermo Fisher Scientific). The culture medium was replaced with fresh medium every 3–4 days. All organoids presented in the manuscript were cultured for at least four weeks before analysis. For sphere growth assay, organoids were washed with PBS, dissociated into smaller pieces, and then treated with siZBTB10 before being resuspended in Matrigel (R&D Systems, Basement Membrane Extract type 2). After Matrigel polymerization, organoid culture medium and 10 μM Y-27632, which inhibits cell dissociation-induced apoptosis, were added to a new 6-well plate. Morphological changes of organoids were monitored using brightfield microscopy and images were taken after 7 days.

Wound healing assay

For wound healing assay, the Culture-Insert 2 well (Ibidi, Germany) was placed into 24-well plates, providing two reservoirs for culturing cells separated by a 500 μm thick wall. Cells were seeded in the reservoirs and cultured until cells attached and formed a monolayer. Upon removal of the silicone inserted from the surface resulted in two precisely defined cell patches, then filled Culture-Insert 2 well with medium. Cell migration was monitored by using live cell imaging and taking photos at different time points.

Cell invasion assay

Matrigel was pre-coated in the transwell chamber (8 μm pores, Corning, USA). Then, 2×10^4 cells in 200μL serum-free medium were added into the upper chambers and 500 μL medium containing 10% FBS was placed in the lower chamber. After 36 h of incubation at 37 °C,

the transwell chambers were taken out, and the cells were fixed in 4% paraformaldehyde solution and stained with 0.1% crystal violet in 20% methanol. Finally, the images were observed and obtained using an inverted microscope.

Immunohistochemical

Two pairs of gastric tumors and adjacent normal tissues obtained from Jiangyin Hospital of Xuzhou Medical University were subjected to formalin fixation, paraffin embedding, and sectioning. The slices were stained with anti-ZBTB10 primary antibodies (1:500, zen-bio, China) and subsequently with the secondary antibody according to the manufacturer's instructions. The immunohistochemistry (IHC) results of intensity scores were analyzed by two pathologists.

Multiplex Immunohistochemical (mIHC)

The formalin-fixed, paraffin-embedded (FFPE) sections were stained with PANO 4-plex IHC kit (Absin Bioscience Inc., Shanghai, China) according to the manufacturer's instructions. Briefly, slides were incubated overnight at 65 °C, deparaffinized in xylene and rehydrated in graded ethanol. The antigen retrieval was carried out with microwave heating, and endogenous peroxidase was quenched using 3% H2O2. The sections were then blocked with 2% bovine serum albumin before incubation with primary antibodies and corresponding followed by HRP-conjugated secondary antibodies and TSA Opal fluorophores staining for each marker. Microwave treatment was used to remove the antibody-TSA complex after each cycle, followed by repeated antigen retrieval, blocking, and primary antibody incubation. Nuclei were stained using DAPI (Sigma, USA). Subsequently, the slides were scanned and imaged using microscopy (Carl Zeiss LSM880, Germany), which captures the fluorescent spectra at 20-nm wavelength intervals from 420 to 720 nm with identical exposure time. Finally, the staining was scored using Zen Analysis software.

The following primary antibodies were used as follows: ZBTB10 (Cat# 163,131, Zenbio, China), CD45 (ab10558, Abcam), CD4 (ab133616, Abcam), CD8 (ab245118, Abcam), EpCAM (sc-66020, Santa).

Statistical analysis

Various R packages and GraphPad Prism 9.0 software were used to visualize statistical analyses. The chi-square test was employed to assess the association between ZBTB10 median expression and clinical features. Normally distributed continuous data were presented as mean ± S.D., and differences between the two groups were compared using the t-test. One-way analysis of variance (ANOVA) was performed to compare differences among multiple groups. For non-normally distributed data, the Mann–Whitney U test was used for two-group comparisons, and the Kruskal–Wallis test was performed for comparisons among multiple groups. Univariate and multivariate Cox regression analyses were performed to measure the hazard ratio (HR), 95% confidence interval (CI) of ZBTB10 expression level, and clinical characteristics of survival. $P < 0.05$ was considered statistically significant.

Result

Transcriptional levels of ZBTB10 in STAD patients

In this study, we evaluated ZBTB10 expression across various cancer types and discovered that ZBTB10 was significantly upregulated in STAD compared to paired normal tissues while low-expressed in several other tumors, suggesting that ZBTB10 may play a distinct role in different cancers (Fig. 1A). Furthermore, with the Encyclopedia of Cancer Cell Lines (CCLE) database, we investigated the relative expression level of ZBTB10 in STAD cell lines (Fig. S1). As shown in the forest plot, univariate Cox regression analysis revealed that high ZBTB10 expression was associated with poor prognosis in STAD patients (Fig. 1B). Collectively, these results indicated that ZBTB10 was upregulated in STAD and may serve as a potential prognostic risk factor.

Upregulation of ZBTB10 correlates with poor prognosis for STAD patients

With TCGA STAD data, we observed that ZBTB10 was significantly overexpressed in tumor tissues than adjacent normal tissues, and this observation was further validated in two independent STAD patient cohorts (GSE54129 and GSE79973) (Fig. 2A-B). Immunohistochemical data from the HPA database demonstrated a trend of higher ZBTB10 protein levels in STAD tissues compared to normal stomach tissues (Fig. 2C, Fig. S2 A). Consistently, we confirmed the elevated protein levels of ZBTB10 in tumors than normal tissues using our collected clinical patient samples (Fig. 2D). Kaplan–Meier survival analysis demonstrated that patients with high ZBTB10 expression exhibited significantly shorter overall survival (OS), disease-specific survival (DSS), and progression-free survival (PFS) in STAD (Fig. 2E-G).

The expression level of ZBTB10 with the clinical pathologic characteristics

The correlation between ZBTB10 mRNA expression and pathological characteristics in STAD samples was analyzed using the UALCAN database, which indicated

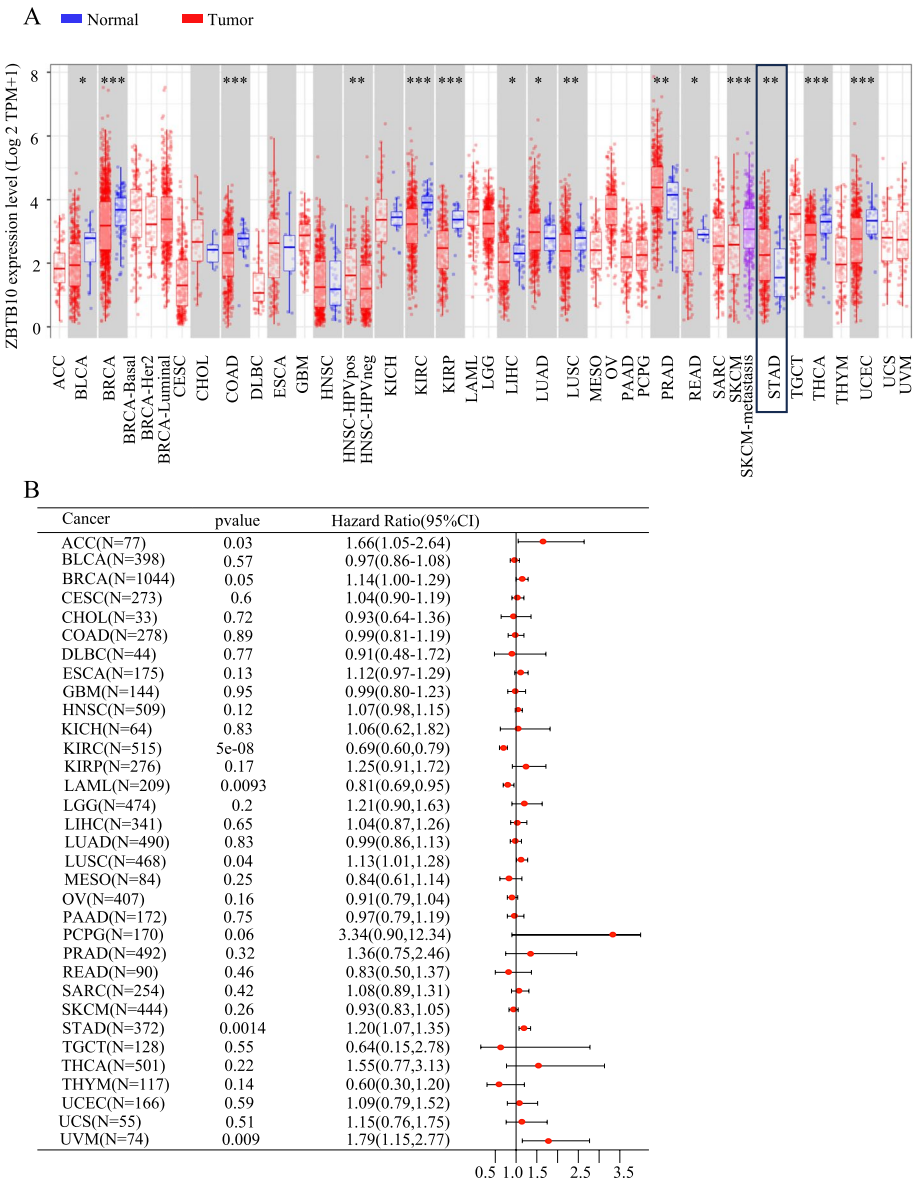

Fig. 1 Expression level of ZBTB10 in human tumors. (**A**) The median mRNA expression levels of ZBTB10 in tumor vs adjacent tissues from the TIMER2 database. (**B**) The forest plot showing the ZBTB10 hazard ratio and poor prognosis in STAD. **P* < 0.05, ***P* < 0.01, ****P* < 0.001

ZBTB10 expression was significantly elevated in STAD patients with higher tumor grade, advanced stage, nodal metastasis, age (41–60 years), and TP53 mutations (Fig. 3A-E). Furthermore, Table S1 also demonstrated that ZBTB10 overexpression in tumor samples was associated with higher T stage, lower expression of TP53, and younger than 65 years old. Additionally, ZBTB10 expression was notably higher in STAD patients without *H. pylori* infection compared to adjacent normal tissues. However, no significant difference

(See figure on next page.)

Fig. 2 Correlation between ZBTB10 expression and survival in STAD patients. (**A_B**) The boxplot showing the the median ZBTB10 mRNA expression level in tumors and their adjacent normal tissues from the GSE54129 and GSE79973 datasets. (**C**) ZBTB10 protein levels in tumor and normal tissues of STAD based on the HPA database. (**D**) Histochemical staining results of ZBTB10 protein expression in tumor and normal tissues from two patients with STAD. Scale bars, 50 μm. (**E–G**) Kaplan–Meier survival analysis of ZBTB10 expression with the overall survival (OS), disease special survival (DSS), and progress free survival (PFS) respectively. Patients were divided into high and low groups based on ZBTB10 median expression. **P* < 0.05, ***P* < 0.01, ****P* < 0.001

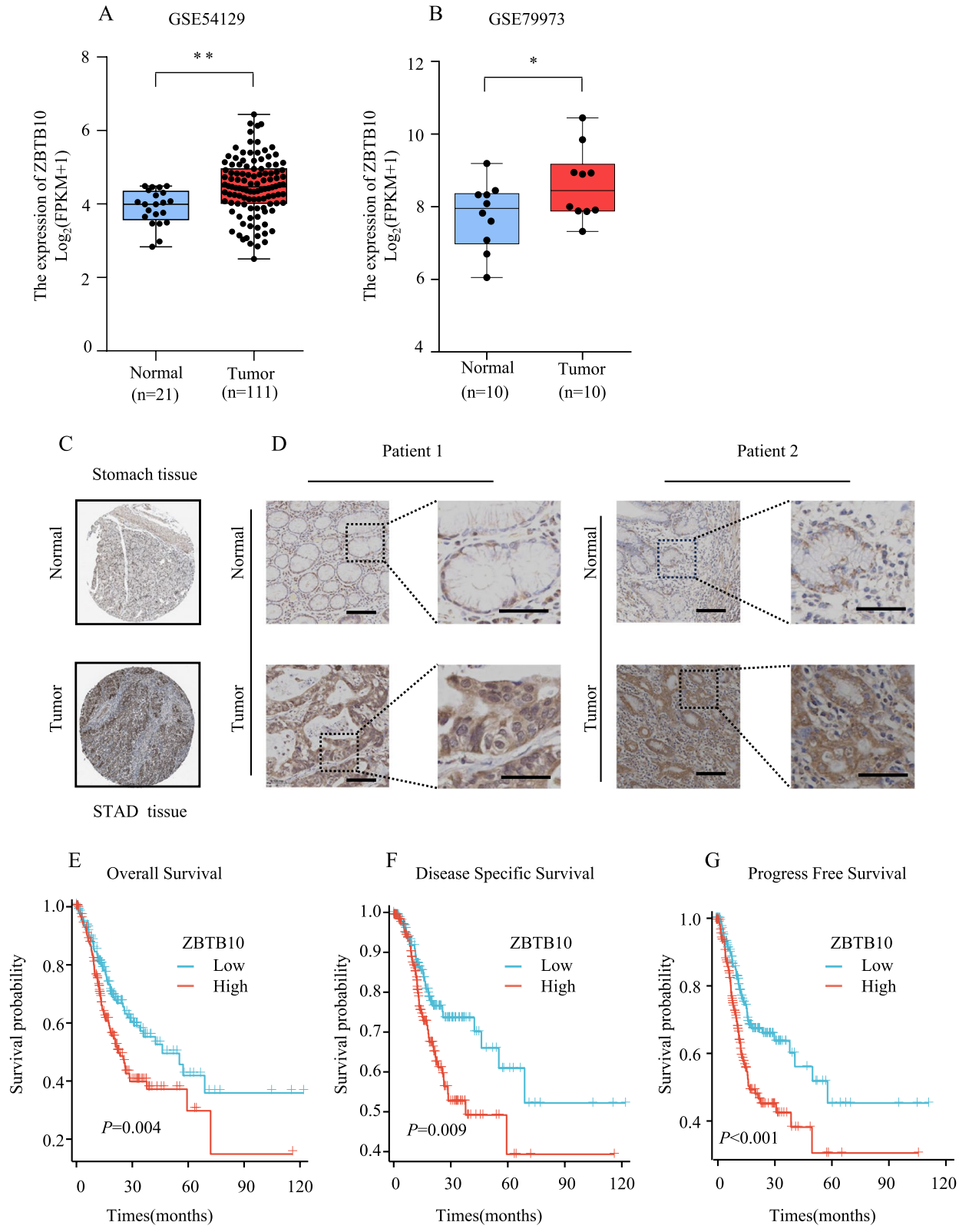

Fig. 2 (See legend on previous page.)

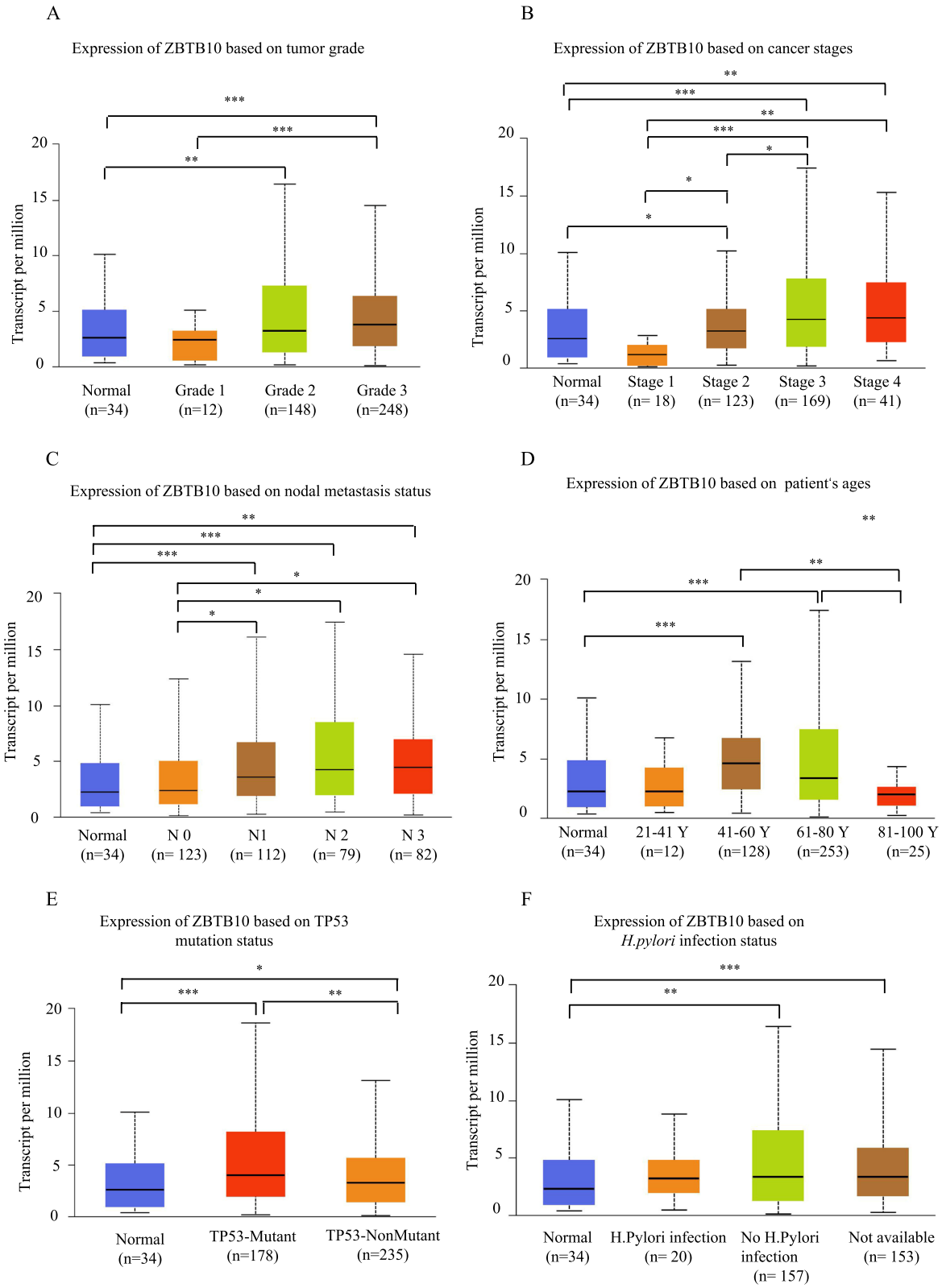

Fig. 3 The clinical characteristics of ZBTB10 expression in STAD tissues. Box-plot showing the ZBTB10 mRNA median expression level correlated with tumor grade (**A**), pathological stages (**B**), lymph node metastases (**C**), patient's ages(**D**), TP53 mutation status (**E**), and *H.pylori* infection status (**F**) respectively. The median expression of ZBTB10 was analyzed using the Mann–Whitney U test for two-group comparisons and the Kruskal–Wallis (**K**-**W**) test for multiple independent groups respectively. *$P < 0.05$, **$P < 0.01$, ***$P < 0.001$

was observed between patients with and without *H. pylori* infection (Fig. 3F, Table S2).

ZBTB10 expression is an independent risk factor for STAD patients

To determine whether ZBTB10 was an independent prognostic factor for STAD patient survival, univariate Cox regression and multivariate Cox regression analysis were performed, which demonstrated that ZBTB10 was an independent prognostic factor for OS in the final multivariable analysis, along with age (Fig. 4A, Table S3). A time-dependent receiver operating characteristic (ROC) curve was performed to evaluate the accuracy of 3-year OS, DSS, and PFS in STAD patients. The area under the curve (AUC) values were 0.602, 0.650, and 0.61, respectively (Fig. 4B-D). In addition, patients in the high-ZBTB10 expression group exhibited a higher probability of death with increasing risk scores (Fig. 4E-G). These findings indicate that ZBTB10 was probably associated with shorter survival. These findings suggested that ZBTB10 may be associated with poorer survival outcomes in STAD.

Correlation of ZBTB10 expression with genetic alterations

Given the abnormal ZBTB10 expression in STAD, we speculated its genetic alterations might contribute to this phenomenon. Therefore, we explore the correlation between ZBTB10 expression and genetic alterations through the cBioPortal database. Amplification was the most common type of copy number alteration (CNA), with a frequency of approximately 5%, while mutation was the second most common alteration observed in TCGA STAD samples (Fig. 5A). Figure 5B illustrated the specific mutation types and locations of ZBTB10 across various cancers, with missense mutations being the predominant genetic alteration. Furthermore, we investigated the potential association between ZBTB10 genetic alterations and the clinical survival prognosis of STAD patients. Interestingly, the data in Fig. 5C–F indicated that STAD patients with ZBTB10 alterations had a worse prognosis in terms of DSS and OS, but not DFS or PFS, compared to patients without ZBTB10 alterations. These findings suggested that the abnormal genetic alterations of ZBTB10 may contribute to the STAD tumorigenesis.

The association of ZBTB10 expression with immune microenvironment

Increasing evidence suggests that tumor mutation burden (TMB) and microsatellite instability (MSI) are closely related to tumor initiation and progression, and can predict the efficacy of tumor immunotherapy. As shown in Fig. 6A-B, ZBTB10 expression was negatively correlated with both TMB and MSI, indicating that higher ZBTB10 expression was associated with a lower mutation status. Next, we analyzed the immunescore and stromalscore using the ESTIMATE algorithm based on ZBTB10 median expression. The results showed that the ZBTB10 low-expression group had significantly higher immunescore and lower stromalscore compared to the high-expression group (Fig. 6C). Immune checkpoints play a critical role in response to cancer immunotherapy, and various immunomodulators including immune stimulators and immune inhibitors might influence the function of infiltrating immune cells. Therefore, the differential expression of immune-regulatory molecules and their correlations between 22 infiltrating immune cells and ZBTB10 expression were further examined using CIBERSORT. The results demonstrated that overexpressed ZBTB10 was strongly associated with higher immune infiltration levels of naive B cells and activated NK cells. In contrast, M1 macrophages, activated memory CD4 + T cells and neutrophils constituted a notably greater proportion in ZBTB10 low-expressed group (Fig. 6D). Additionally, data from the TISIDB database showed that ZBTB10 expression was negatively correlated with the immune cell content of activated CD8 + T cells, activated CD4 + T cells, and activated dendritic cells (DCs) in STAD (Fig. 7A). Among immune stimulators, ZBTB10 expression was negatively associated with CD70, TMIGD2, TNFSF9 and TNFSF13, and similarly negatively correlated with CD274, LIL10RB, LGALS9 and LAG3 among immune inhibitors (Fig. 7B-D). Based on these findings, we reasonably assumed that ZBTB10 expression was primarily associated with the immunosuppressive microenvironments, which was consistent with the poor prognosis in STAD.

Identification of ZBTB10-associated biological function analysis

To investigate the potential downstream mechanism of ZBTB10 in STAD, Gene Ontology (GO) and Kyoto

(See figure on next page.)

Fig. 4 High expression of ZBTB10 indicates poor prognosis in STAD patients. (**A)** The multivariate Cox regression analysis for ZBTB10 median expression and clinical pathological factors in STAD. (**B**-**D)** The receiver operating characteristic (ROC) curve showing the diagnosis value of ZBTB10 3-year overall survival (OS), disease-specific survival (DSS), and progression-free survival (PFS) based on the TCGA STAD database respectively. Patients were divided into high and low groups based on ZBTB10 median expression. (**E**–**F)** Distribution of the survival status between the high-risk and low-risk groups based on ZBTB10 median expression. *$P < 0.05$, **$P < 0.01$, ***$P < 0.001$

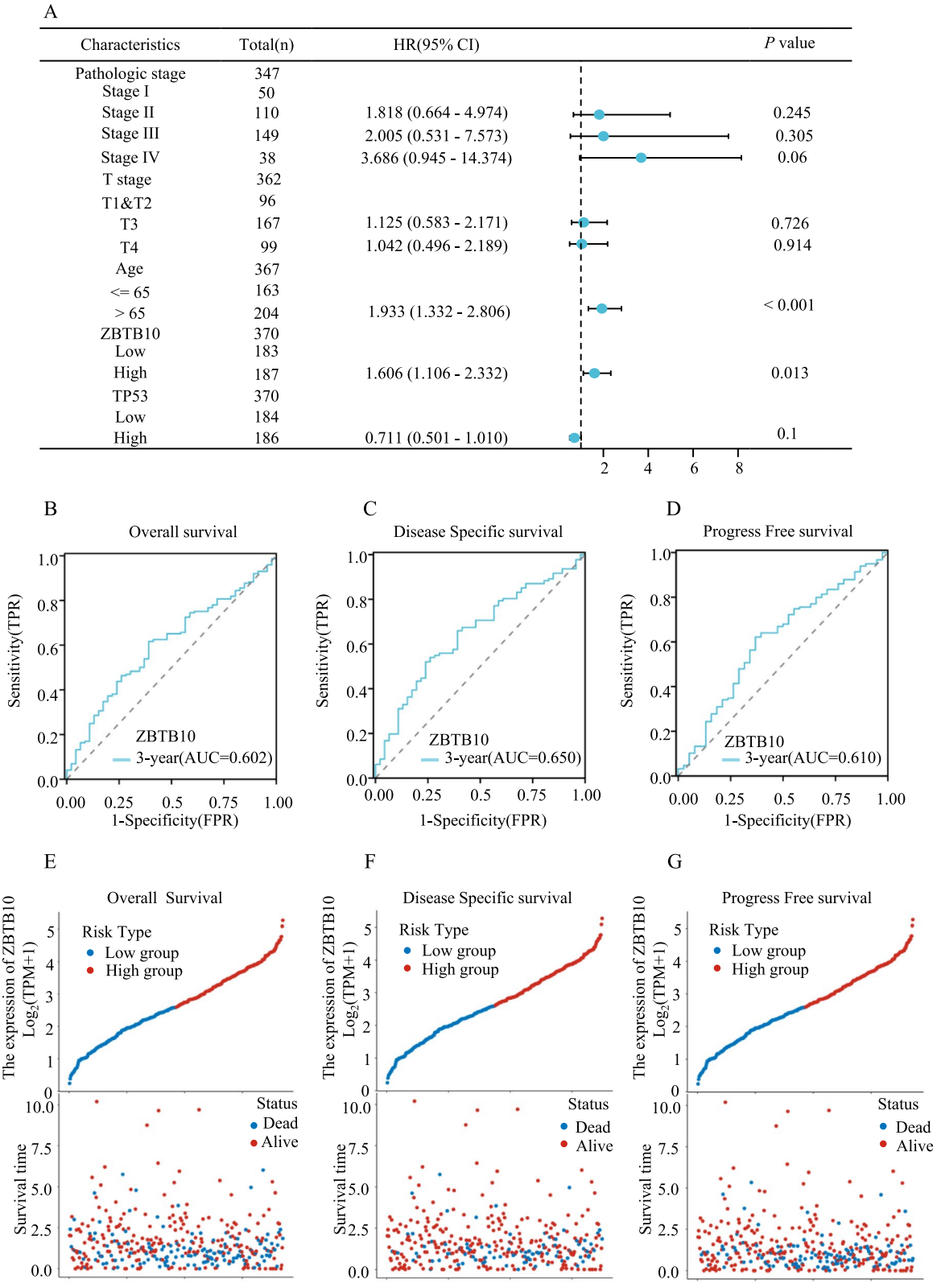

Fig. 4 (See legend on previous page.)

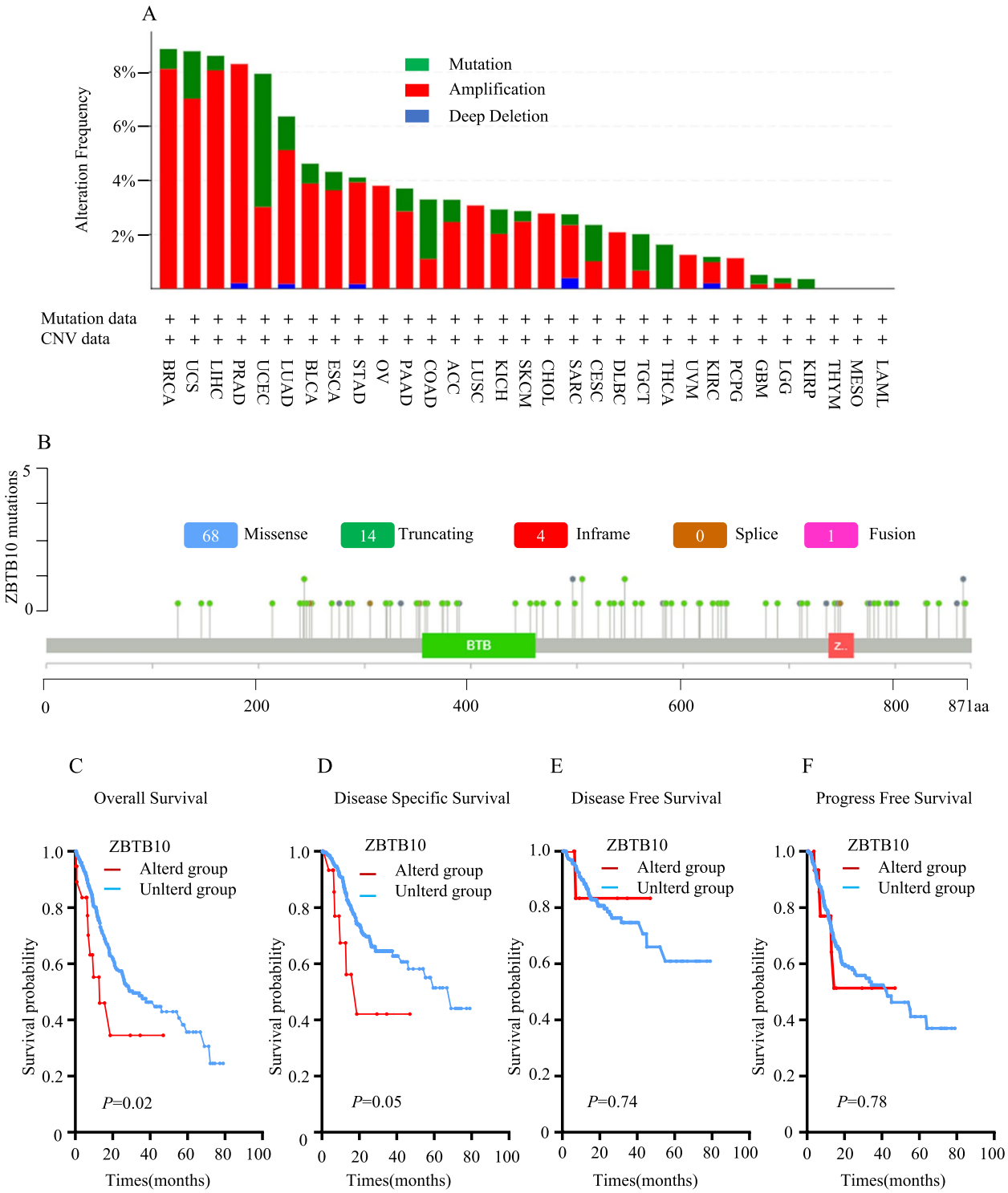

Fig. 5 Genetic alteration characteristics of ZBTB10 across different tumor types.**(A)** The alteration frequency of ZBTB10 mutation type across TCGA tumors using the cBioPortal database. (**B**) The mutation types and locations were displayed. (**C**-**F**) The correlation with overall survival (OS), disease special survival (DSS), disease free survival (DFS) and progress free survival (PFS) based on the mutation status of ZBTB10 in STAD respectively. Patients were divided into high and low groups based on ZBTB10 median expression. $P < 0.05$; $^{**}P < 0.01$; $^{***}P < 0.001$

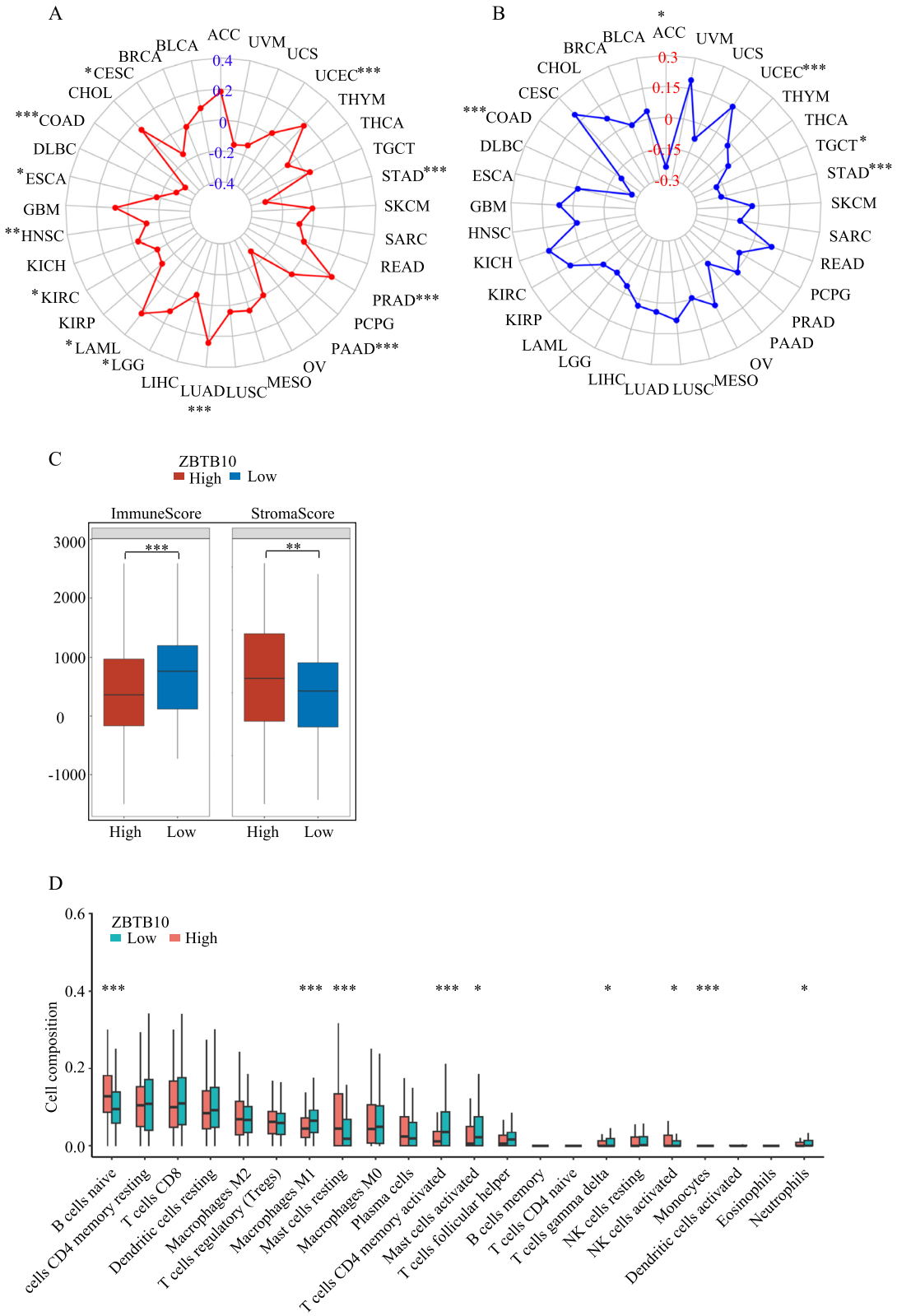

Fig. 6 Correlation of ZBTB10 expression with immune characteristics. (**A**) Radar map displayed the association between ZBTB10 median expression and tumor mutational burden (TMB). (**B**) The radar map displayed the association between ZBTB10 median expression and microsatellite instability (MSI). (**C**) Comparison of immune score and stromal score based on ZBTB10 median expression. (**D**) 22 types of tumor-infiltrating immune cells were analyzed based on ZBTB10 median expression using the CIBERSORT algorithm. *$P < 0.05$, **$P < 0.01$, ***$P < 0.001$

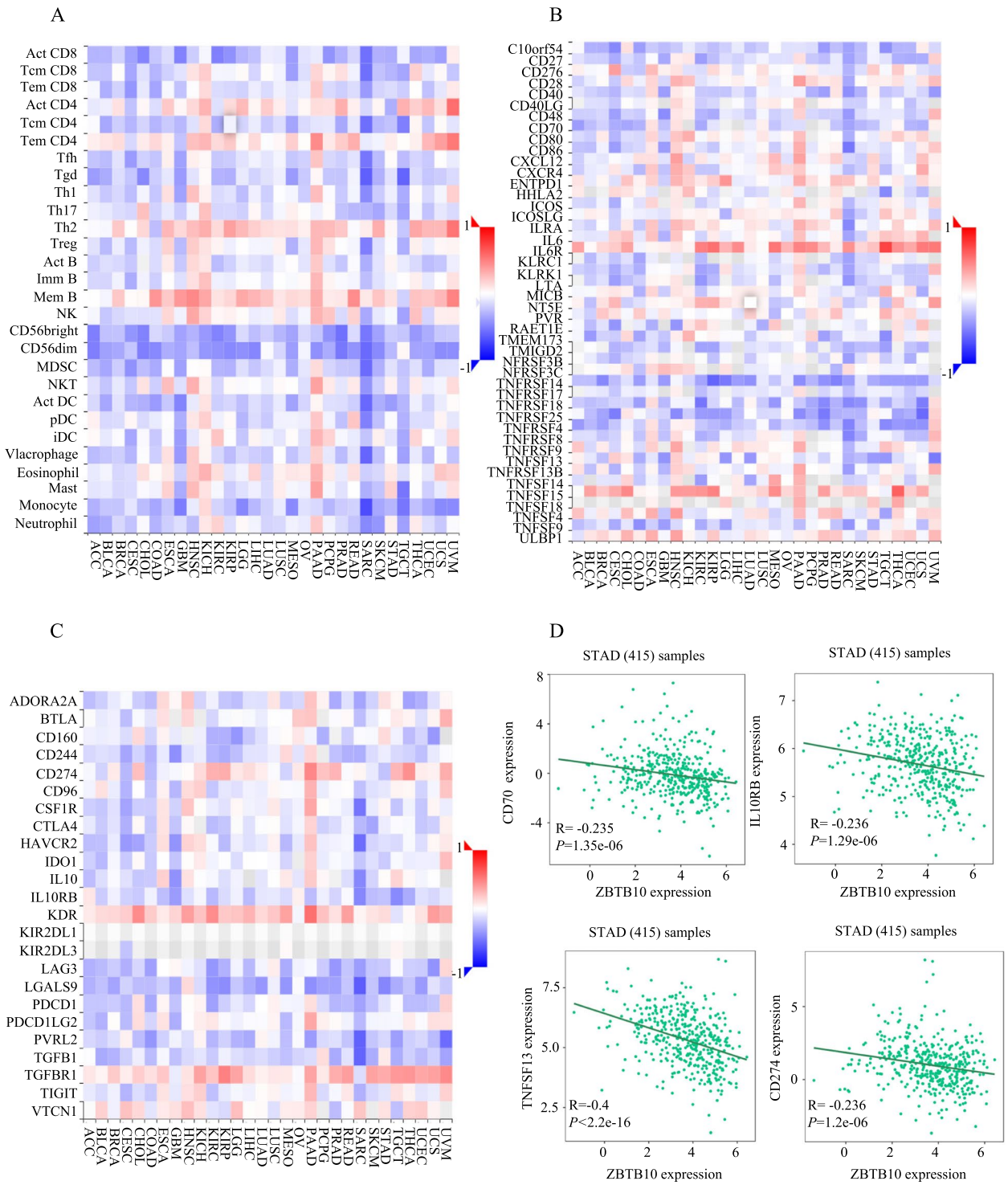

Fig. 7 The association of ZBTB10 expression with tumor immune microenvironment. **(A)** ZBTB10 median expression correlated with tumor-infiltrating lymphocytes. **(B)** ZBTB10 median expression correlated with immune stimulators. **(C)** ZBTB10 median expression correlated with immune inhibitors. **(D)** The correlation analysis of the top four targeting immunosuppressive and immuneactivative markers with ZBTB10 median expression in STAD. **P* < 0.05, ***P* < 0.01, ****P* < 0.001

Encyclopedia of Genes and Genomes (KEGG) analyses were performed based on differentially expressed genes (DEGs) identified between the high and low ZBTB10 expression groups in the TCGA-STAD cohort. GO term analysis revealed that ZBTB10 was strongly associated with extracellular matrix organization, collagen − containing extracellular matrix, and integrin binding (Fig. 8A). KEGG pathway analysis identified several correlated pathways, including ECM-receptor interaction, Cell adhesion molecules, and Calcium signaling pathway (Fig. 8B, Table S4). Furthermore, gene set enrichment analysis (GSEA) based on Hallmarks and KEGG showed that ZBTB10 was positively related to Focal adhesion, MAPK signaling pathway, and PI3 K − Akt signaling pathway. Conversely, the top five negatively correlated pathways of antigen processing and presentation, carbon metabolism, glycolysis/gluconeogenesis, and intestinal immune network for IgA production were shown in Fig. 8C-D. In addition, the top 100 genes co-expressed with ZBTB10 were obtained from the GEPIA2 database, and their protein−protein interaction (PPI) network was visualized using Cytoscape (Fig. 8E). Then, GO analysis displayed that these co-expressed genes were probably involved in the regulation of the cytoskeleton-dependent intracellular transport, cytoplasmic region and cytoskeletal motor activity (Fig. 8F).

The function of ZBTB10 in vitro validation

Given that ZBTB10 was identified as a driver of tumor initiation and progression through our bioinformatics analysis, we selected AGS and MKN-45 cell lines to investigate its role in STAD. RNAi targeting ZBTB10 was then performed for subsequent in vitro experiments. The knockdown efficiency of ZBTB10 mRNA and protein levels were validated by qRT-PCR and Western Blot respectively (Fig. 9A-B). We observed that ZBTB10 knockdown significantly inhibited cell proliferation, and colony formation ability (Fig. 9C-D). Gastric cancer organoids treated with siZBTB10 exhibited a significant decrease in organoid area compared to untreated controls (Fig. 9E). In addition, migration assay showed an obvious reduction of cell migration in both AGS and MKN-45 cells after ZBTB10 knockdown (Fig. 9F). The transwell assay revealed that the invasion ability of ZBTB10 knockdown cells was significantly attenuated compared to controls (Fig. 9G). To evaluate the correlation between leukocyte antigen infiltration and ZBTB10 co-expression, tissue sections from STAD patients were analyzed using multiplexed fluorescence immunohistochemistry (mIHC). We observed a higher percentage of CD45 + T cells/ZBTB10 in tumors as opposed to adjacent normal tissues (Fig. 10). Notably, ZBTB10 expression was negatively correlated with $CD4^+$ and $CD8^+$ T cell infiltration in STAD, consistent with results from both the CIBERSORT and TISIDB databases (Fig. S2B). These findings provide strong evidence that ZBTB10 may play an immunosuppressive role in modulating the tumor immune microenvironment.

Discussion

Previous studies have shown that ZBTB10 is downregulated in breast cancer (BRCA), colon adenocarcinoma (COAD), and nasopharyngeal carcinoma (NPC) tissues, where it acts as a transcriptional inhibitor of SP1 transcription and suppresses tumor activities, including tumor growth, metastasis, and chemoresistance [14, 21, 22]. However, in contrast to previous findings, our results from the TCGA database and IHC analysis revealed that both ZBTB10 mRNA and protein expression levels were elevated in STAD compared to adjacent normal tissues, and that overexpression of ZBTB10 was generally associated with worse survival outcomes. Furthermore, high ZBTB10 expression correlated with increased tumor grade, stages, and lymph node metastasis. Multivariate regression analysis indicated that ZBTB10 was a significant risk factor for the prognosis of STAD patients. Genomic amplification was identified as the predominant type of ZBTB10 alteration, which correlated with worse DSS and OS than patients without these alterations. This amplification may contribute to ZBTB10 overexpression, supporting its potential role as an oncogenic driver in STAD progression. Additionally, mIHC results showed that elevated ZBTB10 protein expression was positively associated with increased infiltration of CD45 leukocyte common antigen (LCA) cells in tumor tissues than normal adjacent tissues. In vitro experiments analysis further revealed that cell proliferation and migration

(See figure on next page.)

Fig. 8 ZBTB10-related genes enrichment analysis and network in STAD. **(A)** GO annotation analysis showed the biological processes, cellular components, and molecular functions based on differentially expressed genes (DEGs) in the TCGA-STAD cohort. **(B)** KEGG pathway analysis was performed based on differentially expressed genes (DEGs) in the TCGA-STAD cohort, and the top eight enriched pathways were visualized using bubble plots. **(C-D)** GSEA with KEGG pathways showed the top five positively and negatively correlated pathways based on differentially expressed genes (DEGs) in the TCGA-STAD cohort. **(E)** The PPI network of ZBTB10-binding proteins was constructed using Cytoscape. Each node was colored according to its degree score, and the circle size represented the extent of interaction for each node. **(F)** GO annotation analysis was performed based on the ZBTB10 co-expressed genes. Patients were divided into high and low groups based on ZBTB10 median expression. $^*P < 0.05$, $^{**}P < 0.01$, $^{***}P < 0.001$

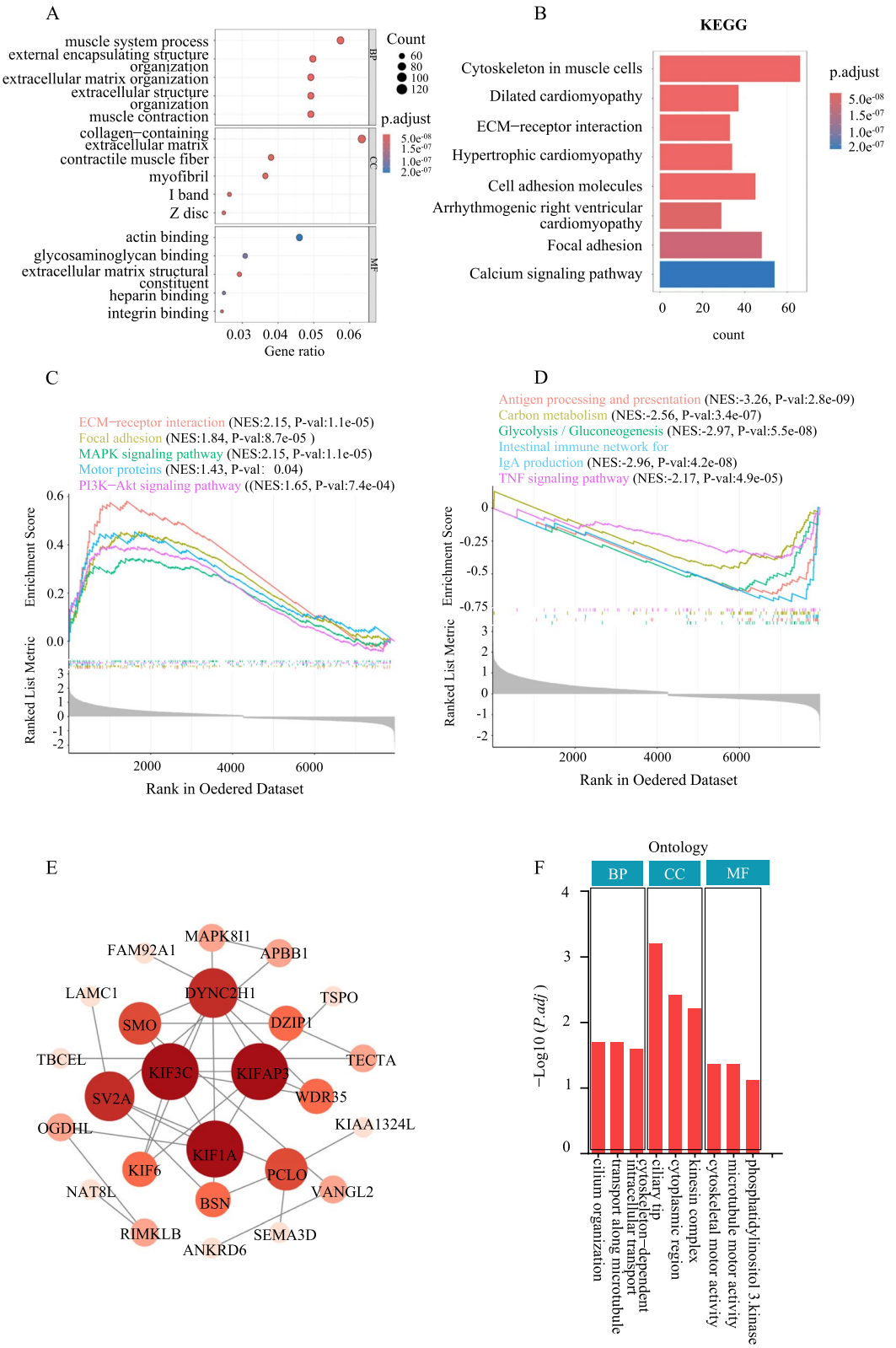

Fig. 8 (See legend on previous page.)

abilities were significantly impaired after the suppression of ZBTB10 in STAD cells. In addition, the inhibition of ZBTB10 significantly reduced the morphological size of gastric cancer organoids. These results are consistent with bioinformatics analysis, which suggested that ZBTB10 was not only an upregulated gene promoting tumor cell development, but also a potential biomarker for predicting the prognosis of STAD patients. Given the relationship between ZBTB10 expression and the tumor immune microenvironment, we performed multiple immune analyses (ESTIMATE, CIBERSORT and TISIDB) to explore the differences in the immune landscape. As expected, ZBTB10 expression was negatively correlated with TMB, MSI, and infiltration of immune cells including M1 macrophages, CD4 + T cells, activated CD8 + T cells, and activated DCs in STAD. Consistent with these analyses, results from mIHC further confirmed that ZBTB10 expression was negatively correlated with $CD4^+$ and $CD8^+$ T cell infiltration in STAD tissues. There is growing evidence that the MSI and TMB status predict the clinical response to immunotherapy in advanced gastric cancer, where high MSI and TMB exhibit an increasing immunosensitive therapy [23, 24]. Furthermore, several studies have demonstrated that M1 macrophages play a crucial role in pro-inflammatory and anti-tumor effects by activating CD8 + T cells and NK cells, thus enhancing their cytotoxicity and killing ability [25–27]. On the other hand, CD8 + T cells are one of key characteristics of secreting cytotoxic molecules, which increase the response to tumor immunotherapy [28, 29]. Subsequent analysis also revealed that ZBTB10 expression was negatively linked to immune stimulators (CD70, TNFSF13) and inhibitors (CD274, IL10RB). Recent studies have shown that the immunosuppressive microenvironment accompanied by low immune status, high abundance of tumor-associated macrophages (TAMs) and cancer-associated fibroblast (CAF) infiltration level, which is consistent with poor prognosis [30–32]. These findings suggest that ZBTB10 was closely related to the "COLD" tumor immune microenvironment, characterized by lower abundances of infiltrating immune cells, thus attenuating the effectiveness of treatment in STAD patients. While high ZBTB10 expression is positively associated with activated NK cells according to the result from CIBERSORT databases, this immune activation may not sufficiently counteract the tumor's intrinsic aggressiveness. Mechanistically, GO and KEGG pathway analysis revealed that ZBTB10 was strongly associated with focal adhesion and ECM − receptor interaction, both of which have been reported to be involved in tumor cell migration and invasion [33–35]. Additionally, GSEA analysis also showed a positive relationship between ZBTB10 and PI3 K-Akt and MAPK signaling pathways. Abnormal activation of the PI3 K-Akt and MAPK pathways plays a key role in regulating cell survival, invasion, and resistance to apoptosis, which are crucial for tumoral activity [36]. Interestingly, our findings contrast with a recent study [37] that showed ZBTB10 expression induced by betulinic acid inhibits gastric cancer progression by inactivating the ARRDC3/ITGB4/PI3 K/AKT pathway, which based on a single-institution patient while our analysis utilized large-scale, publicly available datasets (TCGA and GEO). Furthermore, sequencing platforms and data processing techniques may also contribute to differences in ZBTB10 expression and function. ZBTB10 might exert context-dependent dual functions in tumors—both tumor-suppressive and oncogenic, similar to well-characterized genes such as TP53, Transforming Growth Factor Beta (TGF-β), and C-MYC [38–42]. Therefore, we acknowledge the importance of future studies integrating multi-omics data and larger, independent cohorts to more precisely elucidate the role of ZBTB10 in gastric cancer progression. Besides, based on ZBTB10-coexpressed genes, the results displayed that these differential co-expressed genes participated in biological process such as cilium organization, cytoskeleton-dependent intracellular transport, and triggered microtubule motor activity and cytoskeletal motor activity. Overall, this study investigates the oncogenic characteristics, prognosis of ZBTB10, as well as its significant association with the tumor microenvironment in STAD, suggesting that ZBTB10 may serve as a novel biomarker and therapeutic target for tumor immunotherapy. Although our findings have potential clinical significance, there are several limitations. First, the prognostic and clinicopathological characteristics of ZBTB10 are primarily based on public databases, further study with clinical samples is required to validate these findings. Future studies, including the development of in vivo ZBTB10 mutation-driven phenotype models and the collection of

(See figure on next page.)

Fig. 9 ZBTB10 knockdown inhibits the proliferation and migration in MKN-45 and AGS cell lines. (**A**-**B**) RT-qPCR and Western Blot analysis showed the efficiency of ZBTB10 knockdown in MKN-45 and AGS cells. (**C**) CCK-8 assay showed the proliferation ability after ZBTB10 knockdown at the indicated time points in MKN-45 and AGS cells. (**D**) Colony formation assay showed the number of ZBTB10 knockdown in MKN-45 and AGS cells. (**E**) Brightfield images showed morphological area changes in stomach cancer organoids with or without ZBTB10 knockdown after one week of culture. Scale bar 100 μm. (**F**) Wound healing assay showed the migration ability after ZBTB10 knockdown in MKN-45 and AGS cells. Scale bar 500 μm. (**G**) Transwell assay showed the invasion ability after ZBTB10 knockdown in MKN-45 and AGS cells. The number of invasion cells at 36 h. Three replicates were conducted for each experiment. $^*P < 0.05$, $^{**}P < 0.01$, $^{***}P < 0.001$

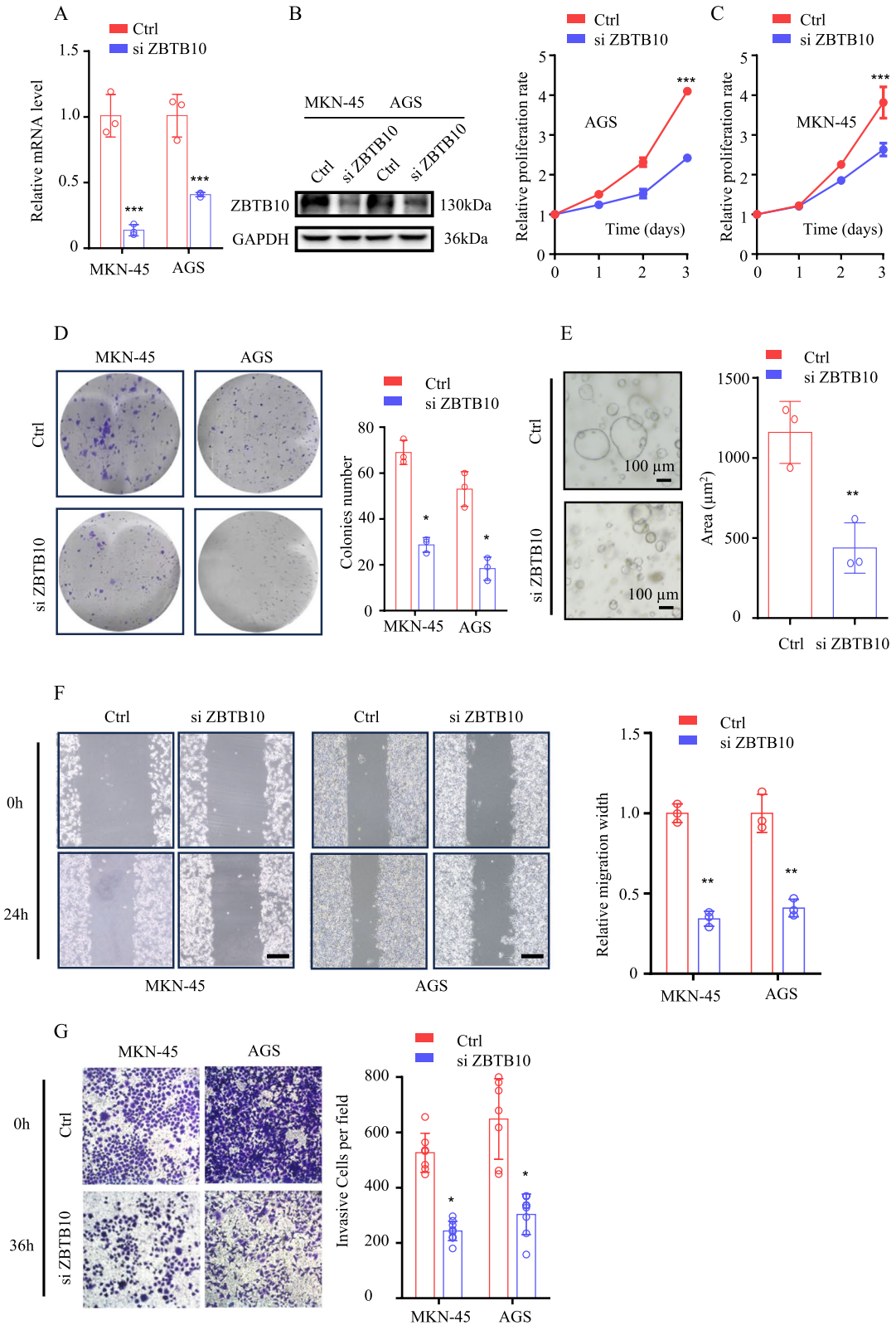

Fig. 9 (See legend on previous page.)

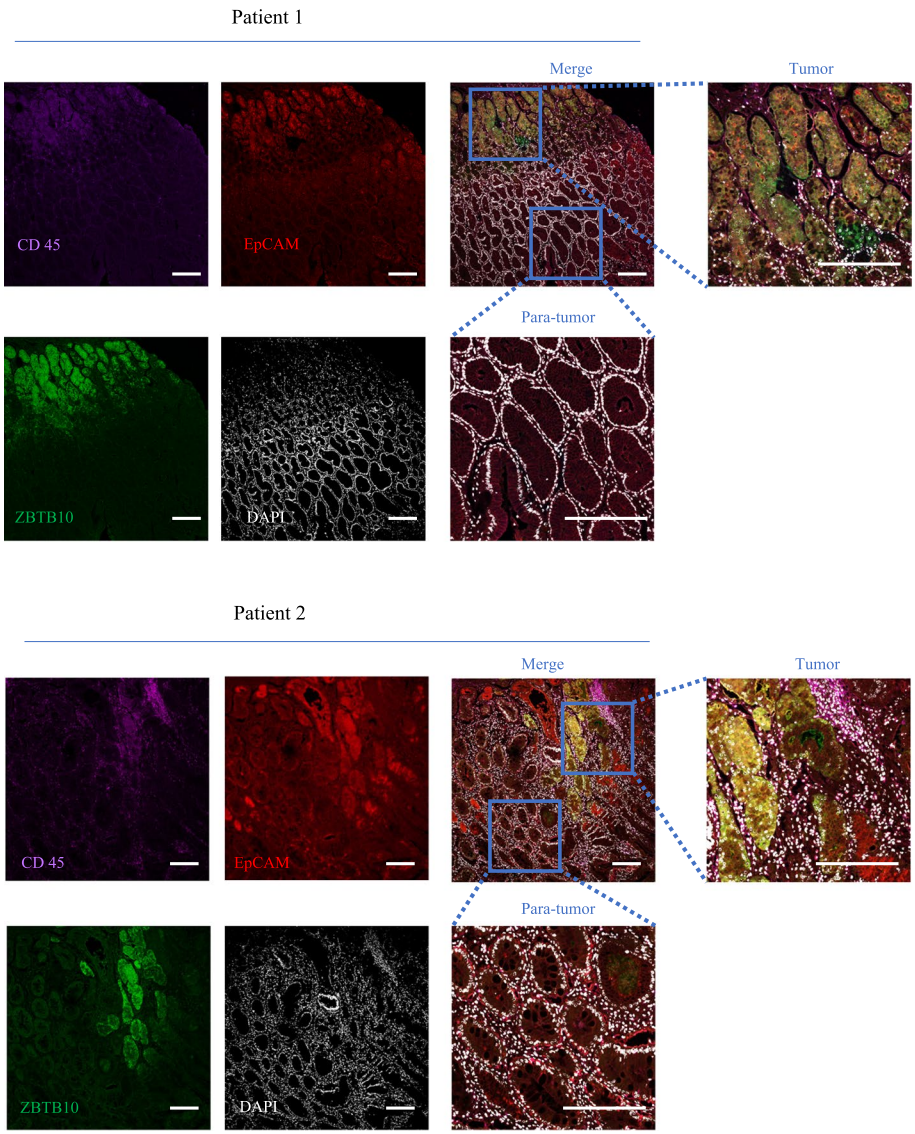

Fig. 10 Multiplex immunohistochemistry (mIHC) staining for identification. Representative mIHC images of STAD tissues and adjacent normal tissues, a staining panel was developed to visualize CD45, EpCAM, ZBTB10 and DAPI simultaneously. CD45: leukocyte marker. EpCAM: epithelial cell marker. Scale bar 200 μm

clinical data on ZBTB10 mutations in STAD patients, will enhance our understanding of the association between ZBTB10 mutations and prognosis. Moreover, further experimental validation is necessary to fully elucidate the detailed molecular mechanism of ZBTB10 in STAD, including analysis of PI3 K-Akt and MAPK pathway components (e.g., Akt, p-Akt, p-ERK) and transcriptome sequencing analysis. Additionally, the immunoregulatory role of ZBTB10 in the tumor microenvironment should be further explored through in vivo/vitro experiments.

Conclusions

In this study, we initially identified that ZBTB10 is markedly upregulated in STAD and correlates with poor prognosis of STAD patients. ZBTB10 could enhance cell proliferation, invasion, and organoid formation in STAD cells. Moreover, our findings demonstrated a significant association between ZBTB10 expression and tumor immune cell infiltration, TMB and MSI, indicating its potential as a diagnostic biomarker and a promising therapeutic target for tumor immunotherapy.

Abbreviations

STAD	Stomach adenocarcinoma
HPA	Human Protein Atlas
TCGA	The Cancer Genome Atlas
TIMER2	Tumor Immune Estimation Resource 2.0
TMB	Tumor mutational burden
MSI	Microsatellite instability
GO	Gene Ontology
GEO	Gene Expression Omnibus
KEGG	Kyoto Encyclopedia of Genes and Genomes
GSEA	Gene Set Enrichment Analysis
mIHC	Multiple Immunohistochemistry

Supplementary Information

The online version contains supplementary material available at https://doi.org/10.1186/s12876-025-04047-y.

Supplementary Material 1.

Acknowledgements
Not applicable.

Authors' contributions
Yingdi Jiang conceived and designed the study. Lu Dai conceived and designed the experiments and methodology. Fuhua Han acquired the data and was responsible for bioinformation analysis. Shali Qiu was responsible for cellular experiments. Yingdi Jiang wrote the original draft. Yanjie Zhou edited and revised the manuscript. Ke Wang and Jiang Lin supervised final manuscript and were responsible for project administration. All authors read and approved the final manuscript.

Funding
This research was supported by the Development Fund of Affiliated Hospital of Xuzhou Medical University (No. XYFY202350).

Data availability
The datasets used and/or analysed during the current study are available from the corresponding author on reasonable request.

Declarations

Ethics approval and consent to participate
The use of human tissues conformed to the guidelines of the Declaration of Helsinki, and this project was approved by the Ethics Committee of the Affiliated Jiangyin Hospital of Xuzhou Medical University (approval number:2020107). The informed consent was obtained from patients involved in the study.

Consent for publication
Not applicable.

Competing interests
The authors declare no competing interests.

Author details
[1]Clinical Laboratory Center, Affiliated Jiangyin Hospital of Xuzhou Medical University, 163 Shoushan Road, Jiangyin, Jiangsu Province 214499, China. [2]Department of Gastrointestinal Surgery, Affiliated Jiangyin Hospital of Xuzhou Medical University, 163 Shoushan Road, Jiangyin, Jiangsu Province 214499, China. [3]Clinical Laboratory Center, Affiliated Guangji Hospital of Suzhou University, 11 Guangqian Road, Suzhou, Jiangsu Province 215003, China. [4]Department of Pathology, Affiliated Jiangyin Hospital of Xuzhou Medical University, 163 Shoushan Road, Jiangyin, Jiangsu Province 214499, China. [5]Traditional Chinese Medicine Orthopedic Hospital, 41 Yunting Middle Street, Jiangyin, Jiangsu Province 214422, China.

Received: 21 October 2024 Accepted: 30 May 2025
Published online: 06 June 2025

References

1. Bray F, Laversanne M, Sung H, et al. Global cancer statistics 2022: GLOBOCAN estimates of incidence and mortality worldwide for 36 cancers in 185 countries. CA Cancer J Clin. 2024;74(3):229–63.
2. Chia N, Tan P. Molecular classification of gastric cancer. Ann Oncol. 2016;27(5):763–9.
3. Yeoh KG, Tan P. Mapping the genomic diaspora of gastric cancer. Nat Rev Cancer. 2022;22(2):71–84.
4. Sexton RE, Al Hallak MN, Diab M, et al. Gastric cancer: a comprehensive review of current and future treatment strategies. Cancer Metastasis Rev. 2020;39(4):1179–203.
5. Sasako M, Sakuramoto S, Katai H, et al. Five-year outcomes of a randomized phase III trial comparing adjuvant chemotherapy with S-1 versus surgery alone in stage II or III gastric cancer. J Clin Oncol. 2011;29(33):4387–93.
6. Cainap C, Vlad C, Seicean A, et al. Gastric cancer: adjuvant chemotherapy versus chemoradiation. A clinical point of view. J Buon. 2019;24(6):2209–19.
7. Zhu L, Wang H, Jiang C, et al. Clinically applicable 53-gene prognostic assay predicts chemotherapy benefit in gastric cancer: a multicenter study. EBioMedicine. 2020;61:103023.
8. Bu S, Lv Y, Liu Y, et al. Zinc finger proteins in neuro-related diseases progression. Front Neurosci. 2021;15: 760567.
9. Karunasinghe N. Zinc in prostate health and disease: a mini review. Biomedicines. 2022;10(12):3206.
10. Liu S, Sima X, Liu X, et al. Zinc finger proteins: functions and mechanisms in colon cancer. Cancers (Basel). 2022;14(21):5242.
11. Zhang Z, Wu L, Li J, et al. Identification of ZBTB9 as a potential therapeutic target against dysregulation of tumor cells proliferation and a novel biomarker in liver hepatocellular carcinoma. J Transl Med. 2022;20(1):602.
12. Liu S, Liu X, Lin X, et al. Zinc finger proteins in the war on gastric cancer: molecular mechanism and clinical potential. Cells. 2023;12(9):1314.
13. Wang S, Xu Z, Li M, et al. Structural insights into the recognition of telomeric variant repeat TTGGGG by broad-complex, tramtrack and bric-à-brac - zinc finger protein ZBTB10. J Biol Chem. 2023;299(3):102918.
14. Liu X, Jutooru I, Lei P, et al. Betulinic acid targets YY1 and ErbB2 through cannabinoid receptor-dependent disruption of microRNA-27a:ZBTB10 in breast cancer. Mol Cancer Ther. 2012;11(7):1421–31.
15. Li X, Pathi SS, Safe S. Sulindac sulfide inhibits colon cancer cell growth and downregulates specificity protein transcription factors. BMC Cancer. 2015;15:974.
16. Lai Y, Zhang X, Zhang Z, et al. The microRNA-27a: ZBTB10-specificity protein pathway is involved in follicle stimulating hormone-induced VEGF, Cox2 and survivin expression in ovarian epithelial cancer cells. Int J Oncol. 2013;42(2):776–84.
17. Smita S, Ghosh A, Biswas VK, et al. Zbtb10 transcription factor is crucial for murine cDC1 activation and cytokine secretion. Eur J Immunol. 2021;51(5):1126–42.
18. Yoshihara K, Shahmoradgoli M, Martínez E, et al. Inferring tumour purity and stromal and immune cell admixture from expression data. Nat Commun. 2013;4:2612.
19. Yan HHN, Siu HC, Law S, et al. A comprehensive human gastric cancer organoid biobank captures tumor subtype heterogeneity and enables therapeutic screening. Cell Stem Cell. 2018;23(6):882-897.e811.
20. Seidlitz T, Merker SR, Rothe A, et al. Human gastric cancer modelling using organoids. Gut. 2019;68(2):207–17.
21. Pang MJ, Yang Z, Zhang XL, et al. Physcion, a naturally occurring anthraquinone derivative, induces apoptosis and autophagy in human nasopharyngeal carcinoma. Acta Pharmacol Sin. 2016;37(12):1623–40.
22. Fosso E, Leo M, Muccillo L, et al. Quercetin's dual mode of action to counteract the Sp1-miR-27a axis in colorectal cancer cells. Antioxidants (Basel). 2023;12(8):1547.
23. Picard E, Verschoor CP, Ma GW, et al. Relationships between immune landscapes, genetic subtypes and responses to immunotherapy in colorectal cancer. Front Immunol. 2020;11: 369.

24. Cheng Y, Bu D, Zhang Q, et al. Genomic and transcriptomic profiling indicates the prognosis significance of mutational signature for TMB-high subtype in Chinese patients with gastric cancer. J Adv Res. 2023;51:121–34.
25. Farhood B, Najafi M, Mortezaee K. CD8(+) cytotoxic T lymphocytes in cancer immunotherapy: a review. J Cell Physiol. 2019;234(6):8509–21.
26. Zhao C, Pang X, Yang Z, et al. Nanomaterials targeting tumor associated macrophages for cancer immunotherapy. J Control Release. J2022;341:272–84.
27. Li D, Xia L, Huang P, et al. Cancer-associated fibroblast-secreted IGFBP7 promotes gastric cancer by enhancing tumor associated macrophage infiltration via FGF2/FGFR1/PI3K/AKT axis. Cell Death Discov. 2023;9(1):17.
28. Park J, Hsueh PC, Li Z, et al. Microenvironment-driven metabolic adaptations guiding CD8(+) T cell anti-tumor immunity. Immunity. 2023;56(1):32–42.
29. Ding JT, Yang KP, Zhou HN, et al. Landscapes and mechanisms of CD8(+) T cell exhaustion in gastrointestinal cancer. Front Immunol. 2023;14:1149622.
30. Luo Q, Dong Z, Xie W, et al. Apatinib remodels the immunosuppressive tumor ecosystem of gastric cancer enhancing anti-PD-1 immunotherapy. Cell Rep. 2023;42(5):112437.
31. Li D, Huang P, Xia L, et al. Cancer-associated fibroblasts promote gastric cancer cell proliferation by paracrine FGF2-driven ribosome biogenesis. Int Immunopharmacol. 2024;131:111836.
32. Saigí M, Mesía-Carbonell O, Barbie DA, et al. Unraveling the intricacies of CD73/adenosine signaling: the pulmonary immune and stromal microenvironment in lung cancer. Cancers (Basel). 2023;15(23):5706.
33. Cicchini C, Laudadio I, Citarella F, et al. TGFbeta-induced EMT requires focal adhesion kinase (FAK) signaling. Exp Cell Res. 2008;314(1):143–52.
34. Qin S, Guo Q, Liu Y, et al. A novel TGFbeta/TGILR axis mediates crosstalk between cancer-associated fibroblasts and tumor cells to drive gastric cancer progression. Cell Death Dis. 2024;15(5):368.
35. Li D, Xia L, Huang P, et al. Heterogeneity and plasticity of epithelial-mesenchymal transition (EMT) in cancer metastasis: focusing on partial EMT and regulatory mechanisms. Cell Prolif. 2023;56(6):e13423.
36. Morgos DT, Stefani C, Miricescu D, et al. Targeting PI3K/AKT/mTOR and MAPK signaling pathways in gastric cancer. Int J Mol Sci. 2024;25(3):1848.
37. Huang Z, Li Y, Zhao Z, et al. Enhanced ZBTB10 expression induced by betulinic acid inhibits gastric cancer progression by inactivating the ARRDC3/ITGB4/PI3K/AKT pathway. Cell Oncol (Dordr). 2025;48(3):675-692
38. Shen J, Zhao DS, Li MZ. TGF-β1 promotes human gastric carcinoma SGC7901 cells invasion by inducing autophagy. Eur Rev Med Pharmacol Sci. 2017;21(5):1013–9.
39. Won KY, Kim GY, Kim HK, et al. The expression of C-MYC in gastric adenocarcinoma is associated with PD-L1 and FOXP3 expression: C-MYC overexpression is a good prognostic factor. Pathol Res Pract. 2019;215(11):152639.
40. Zhang L, Hou Y, Ashktorab H, et al. The impact of C-MYC gene expression on gastric cancer cell. Mol Cell Biochem. 2010;344(1–2):125–35.
41. Veen LM, Skrabanja TLP, Derks S, et al. The role of transforming growth factor β in upper gastrointestinal cancers: a systematic review. Cancer Treat Rev. 2021;100:102285.
42. Muller PA, Vousden KH. Mutant p53 in cancer: new functions and therapeutic opportunities. Cancer Cell. 2014;25(3):304–17.

Publisher's Note